Regular Article

Malek Ali*, Abderraouf Gherissi and Yousef Altaharwah

Experimental and simulation study on a rooftop vertical-axis wind turbine

https://doi.org/10.1515/eng-2022-0465
received January 14, 2023; accepted May 08, 2023

Abstract: In this study, a small vertical-axis wind turbine (VAWT) was successfully designed and tested to produce electrical energy using renewable wind energy after being installed on the roof of buildings. The VAWT was constructed according to the existing wind source in the Tabuk region in Saudi Arabia. The use of VAWT on roofs is a sustainable solution for producing clean electricity and contributing to a portion of the local electricity consumption. A rooftop wind turbine test was performed to determine the behavior and output of a VAWT under non-constant wind speeds under natural conditions. To verify the resistance of the shear stress and pressure, a computational fluid dynamics (CFD) simulation on the airfoil was conducted. The experimental test results showed that the VAWT can reach its rated power at 9 m/s. The minimum wind speed needed for power production was 3 m/s. The maximum power coefficient obtained during testing was approximately 0.45 at a tip speed ratio of around 1.94. The simulation mesh is constructed with Ansys mesh. Two dimensional (2-D) mapped face meshing, fine, high smoothing mesh was constructed with 50 division numbers and a bias factor of about 150. The grid with 15,000 cells generated the same results as the higher number of cell grids. The simulation equivalent force was about 2.8 N for a single blade, such as 8.5 N in total, which presents an error of about 3%. The CFD simulation and experimental tests on existing forces confirm that the VAWT structure's resistance can be guaranteed at high wind speeds.

Keywords: rooftop vertical-axis wind turbine, H-Darrieus wind turbine, tip speed ratio, power coefficient, CFD simulation

Notation

C_p	power coefficient
CFD	computational fluid dynamics
D	diameter of the turbine (m)
E	wind energy (J)
F_D	drag force (N)
F_L	lift force (N)
F_N	normal force (N)
F_T	tangential force (N)
HAWT	horizontal-axis wind turbine
I	electrical current (A)
L	blade length (m)
M	air mass (kg)
$\dot{M}$	air mass flow rate (kg/s)
P_E	electrical power (W)
P_{Mech}	mechanical power (W)
P_w	wind power (W)
T	torque (N m)
$\overrightarrow{U}$	velocity (m/s)
V	electrical voltage (V)
VAWT	vertical-axis wind turbine
$\overrightarrow{V}$	tangential velocity (m/s)
V_b	speed of the tips of turbine blades (m/s)
V_w	velocity of the wind (m/s)
$\overrightarrow{W}$	relative velocity (m/s)
α	angle of attack (deg)
λ	tip-speed-ratio
∞	azimuthal angle (deg)
Ω	angular frequency (rad/s)
ρ	air density (kg/m^3)
ω	angular velocity of the rotor (1/s)

*** Corresponding author: Malek Ali,** Aircraft Maintenance Department, Faculty of Aviation Sciences, Amman Arab University, Amman, 11953, Jordan, e-mail: m.alsalem@aau.edu.jo, tel: +962-79-0851286
Abderraouf Gherissi: Mechanical Engineering Department, Faculty of Engineering, University of Tabuk, P.O. Box 741, Tabuk 71491, Saudi Arabia
Yousef Altaharwah: Renewable Energy Engineering Department, Faculty of Engineering, Amman Arab University, Amman, 11953, Jordan

1 Introduction

Owing to the price instability of fossil fuels globally for political or non-political reasons, wind energy is an important renewable and sustainable energy resource that is widely used as an alternative energy source. The most important advantages of renewable energy are lower costs as well as lower non-carbon emissions, and this makes renewable energy friendly to the climate and environmentally friendly. There are two main types of renewable energy: solar energy and wind energy. Both types are widely used as sources of electric power generation. The global focus on wind energy conversion has increased with horizontal-axis wind turbine (HAWT) and vertical-axis wind turbine (VAWT).

Wind power was shown to have the lowest relative greenhouse gas emissions, the least water consumption demands, and the best social consequences; yet, it takes more acreage and has a higher relative capital cost [1]. Several factors affect the performance and life cycle of the VAWT [2–4]. Experiments indicated that an HAWT outperformed a VAWT under the same meteorological conditions in terms of performance and shorter wake (faster recovery) [5]. Experimental research was done on the effectiveness, drag, and horizontal midplane wake characteristics of a vertical-axis Savonius wind turbine, based on the findings from the wake measurements, and some recommendations on where to place supplementary turbines are made [6]. The wind conditions on the roof and the behavior of a roof-located wind turbine with respect to optimized energy yield were addressed by Sander et al. [7], and it was concluded that an H-Darrieus is preferred to the HAWT for operation on a flat roof of higher buildings. [8] How the remaining lifetime of a wind turbine component can be estimated based on online measurement data was investigated, and it was found from the interviews that the owners do not get sufficient information from the manufacturer in order to do similar studies [9]. By analyzing the link between the aspect ratio of a vertical-axis straight-bladed (H-Rotor) wind turbine and its performance (power coefficient), the numerical study employed demonstrated how the Reynolds number of rotor blades has a significant impact on the turbine performance. From a geometrical perspective, as the aspect ratio decreases, the Reynolds number increases, enhancing the performance of wind turbines [10]. The Darrieus VAWT configurations were evaluated, including the drawbacks of each variation that hindered the development into a large-scale rotor.

The blade is the most important component of any wind turbine; the airfoil of the blade must be carefully designed in order to achieve the best energy output. Blade section simulations were carried out for the S822 airfoil at a chord Reynolds number of 100,000 and an angle of attack of 5°. The simulations provide insights into a physical mechanism that explains the lift increase observed for rotating blade sections when compared with stationary blade sections, which is commonly referred to as rotational augmentation [11]. XFOIL was used to develop and test three high-performance airfoils (EYO7-8, EYO8-8, and EYO9-8) for small wind turbine applications in the study of Emmanuel et al. [12]. Preliminary wind turbine rotor analysis also showed that EYO7-8, EYO8-8, and EYO9-8 rotors had maximum power coefficients of 0.371, 0.366, and 0.358, respectively. A proposal for a new design criterion for H-Darrieus turbines based on the energy-yield maximization was given in the study of Bianchini et al. [13]; critical analysis of the best design choices in terms of turbine shape, dimensions, airfoils, and constraints was clarified. A comparison of NACA 6-series and 4-digit airfoils for Darrieus wind turbines was done by Migliore [14], and ten different airfoils having thickness-to-chord ratios of 12, 15, and 18% were studied. Performance estimates were made using a blade element/momentum theory approach. The results indicated that NACA 6-series airfoils show peak power coefficients as great as NACA 4-digit airfoils and have broader and flatter power coefficient/tip speed ratio curves. The design life of wind turbines is often about 20 years. In practice, it is often noted that the components in the turbine fail earlier and must be replaced before the advertised age. Therefore, it is very important for wind turbine owners to have a good assessment of the remaining components and develop an appropriate maintenance schedule. Wind turbines must follow a technical standard that provides common rules and guidelines. This standard specifies the basic design requirements for wind turbines, which include protocols for engineering design and component testing. The standard is implemented to provide an adequate level of protection against damage to turbines and their subsystems. Implementing standards in the turbine design process is an important part. It is critical to consider the external conditions when designing the wind turbine because it is dependent on the location where it is built.

In this study, a small-scale VAWT was created in order to reduce the home electrical energy budget charge and take advantage of the majority of urban building top roofs that are empty. Moreover, based on the average wind speed in the Tabuk region of Saudi Arabia, the wind turbine was designed with an H-Darrius NACA 0018 airfoil. A complete design was created to generate and measure the mechanical and electrical power output

from the VAWT under real-world wind speed conditions. The turbine was tested in the Tabuk region at different wind speeds. Several studies have been conducted on the performance of VAWTs. In contrast to previous studies, the focus here will be on wind speed and airfoil simulation.

2 Experimental method

This experimental and simulation study aimed to investigate natural wind effects on VAWT modules in the Tabuk region in Saudi Arabia and to test different wind speeds and their corresponding power coefficient. In this study, VAWTs were tested on the roof of buildings. The power coefficient (C_p) was calculated based on both the wind power (P_w) and mechanical power (P_{Mech}). An Anemometer (RM Young 03002L) was used to measure the wind velocity (V_w) with ±0.5 m/s accuracy. The electrical power (P_E) was calculated by equation (8). The electrical voltage (V) and current (I) were measured by a digital multimeter (Fluke 179 True-RMS Digital Multimeter) with ±(0.09% + 2) voltage (V) accuracy and ±(1.0% + 3) current (I) accuracy, resulting in power uncertainty of $[V^2(\pm(1.0\% + 3)^2) + I^2(\pm(0.09\% + 2)^2)]^{1/2}$ [15]. A high-precision torque sensor (Kistler Dual Range Torque Sensor 4503B) was used for measuring the dynamic torque and rotational speed on the turbine shaft. The measurement range of the torque sensor is 10 N m with an accuracy of 0.1% of its full-scale range. The linearity error including the hysteresis of the torque sensor is less than ±0.1% of the rated torque. All measurements from the sensor (torque and rotational speed) were recorded at a sampling rate of 135 Hz by using a USB DAQ connected to a computer.

Experiment data were analyzed in order to calculate the power coefficient. A comparative assessment for different wind speeds was done to distinguish the rated power that suits VAWT specifications. The experimental and simulation results of the study were matching.

2.1 VAWT design

The design of the blade and its airfoil was based on several previous studies. The computer-aided design (CAD) of VAWT is shown in Figure 1.

VAWT was successfully designed from the main parts of the prototype as listed in Table 1.

Aluminum was chosen for the blades because it is lightweight and resistant to corrosion. In addition, composite

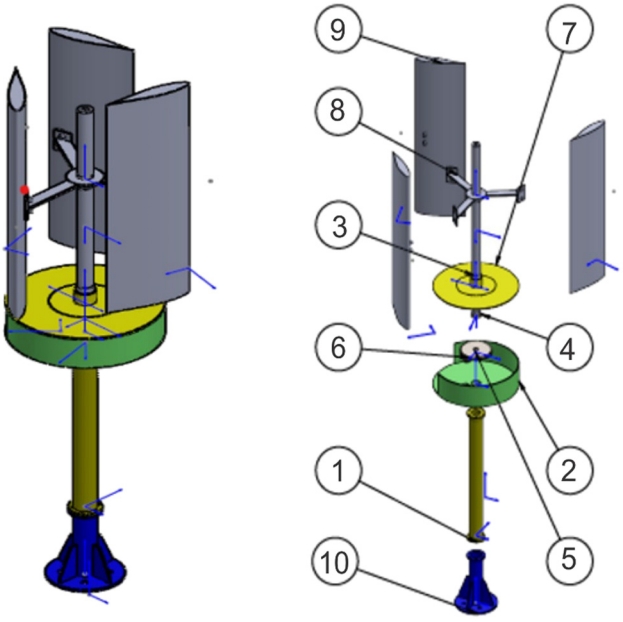

Figure 1: CAD design of the VAWT with it's main parts.

materials that are based on aluminum, epoxy, or plastic can be used and are usually reinforced with different types of reinforcements, such as titanium carbide or natural fibers, among others. The improvement of the composite surface hardness by air abrasive jet polishing of SiO_2 particles was done in the study of Gherissi and Ali [16]. The obtained results demonstrated the importance of superficial hardening of composites Al-TiC by the impact of the SiO_2 air jet and show that the surface hardness improvement is greatest for the nanocomposites compared with microcomposites and a pure matrix material. In the study of Ali and Gherissi [17], aluminum matrix composites were successfully synthesized by melting the Al scrap at 850°C. It was observed that the ultimate tensile strengths of Al-SiO_2 composites with 0, 10, and 20 wt% of SiO_2 were 25, 62, and 65 MPa, respectively. The epoxy matrix composites

Table 1: Main parts of the VAWT

Item no.	Part number	Quantity
1	Tower	1
2	Container	1
3, 6	Ball bearing	2
4	Shaft	1
5	Spur gear	2
7	Plate	1
8	Arms (rotor)	1
9	Blade	3
10	Base	1

reinforced with various concentrations of titanium carbide (TiC) have been synthesized and characterized successfully in the study of Ali [18]; the results obtained show improvements in both the mechanical and tribological behavior of the composites. The other parts were made from steel to withstand fatigue and give more stability to the whole prototype. The blade design was changed from a solid cross section to a hollow cross section with various wall thicknesses in order to reduce both mass and centrifugal forces on the blades. The maximum stresses and maximum deflection must be proportional to the thickness of the wall. It was found that the solid cross section has the maximum stress and deflection, so it was chosen for the design of the VAWT.

The speed and kinetic energy of the wind must be reduced in order to extract the required energy. Several studies have found that if too much wind energy is excluded, the wind is on the downwind flank of the VAWT. This phenomenon would then cause compression in front of the blades and a slight blow-off on the flank sides rather than turning the blades, resulting in a power limit for the VAWT. The VAWT will then operate between 50 and 60% of its theoretical maximum efficiency due to blade efficiency, generator efficiency, friction losses, and electrical losses. In addition, if the wind speed exceeds the furling velocity, the wind turbine has to be shut down to prevent the blades from breaking. A mechanical brake is then required for the wind turbine rotor's safety. To ensure sufficient speed at the generator side, a gearbox was designed that can accelerate a rotational speed at a ratio of about 5.7; that is, every time the blades make one revolution, the generator shaft spins 5.7 times.

The experiments were conducted on the vertical wind turbine prototype shown in Figure 2. The wind turbine performance was carried out under several wind conditions, as shown in Table 2. The maximum wind speed was about 13 m/s and the lowest was 3 m/s. The optimum tilt angle was established by determining the wind direction and the maximum output rotational speed of the rotor. The actual measured energy is calculated as input mechanical force and output electrical energy.

The airfoil was selected as NACA 0018 based on several previous studies. Because of its resistance to changes in the angle of attack and wind speed, the NACA 0018 airfoil typically provides more lift, has fewer manufacturing constraints, and has greater sustainability and fatigue resistance. The wind blade, the airfoil NACA 0018, and the applied forces are shown in Figure 3. Different aerodynamic forces can be generated on the sectional profile of the blades due to the airflow stream through the turbine rotors. Mainly, these forces are the drag force F_D and the lift force F_L: the drag force in the direction of the airflow and the lift force

Figure 2: VAWT prototype with 1 m three-blade H-Darrieus.

perpendicular to the airflow. When optimizing wind turbine blades, the goal is to maximize the lift force while minimizing the drag force. As the turbine rotates, the airfoil's angle of attack α continuously changes as a function of its azimuthal position θ, which produces variable aerodynamic forces and is often referred to as the Darrieus motion [19]. The magnitude and orientation of the lift and drag forces as well as the resultant force vary. The resultant force can be decomposed into a normal force F_N and a tangential force F_T. The tangential force component then drives the rotation of the wind turbine and produces the torque necessary to generate electricity [20].

A computational fluid dynamics (CFD) simulation was conducted on the ANSYS student version of the airfoil at a wind velocity (10 m/s), which matched

Table 2: Experimental VAWT testing results on natural wind speeds

V_w (m/s)	3	5.4	6.8	7.3	8	9	10
N_{rotor} (rpm)	40	120	200	220	300	450	540
V_b (m/s)	1.55	4.65	7.75	8.53	11.63	17.44	20.93
λ	0.52	0.87	1.14	1.17	1.46	1.94	2.1
T (N m)	0.25	1.25	2	2.8	3	3.1	3.2
P_{Mech} (W)	1.05	15.71	41.89	64.51	94.25	146.09	180.96
C_p	0.09	0.23	0.3	0.37	0.41	0.45	0.4

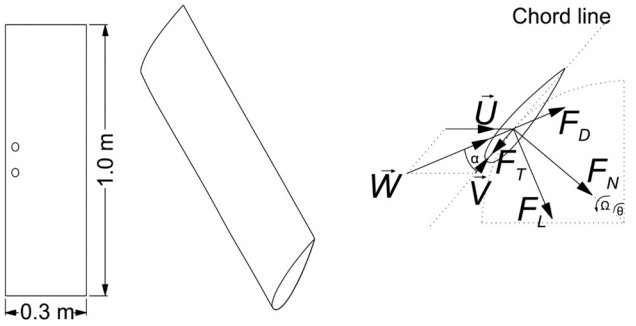

Figure 3: The wind blade, the airfoil NACA 0018, and applied forces.

the maximum experimental wind speed reached in the experiments.

3 Results and discussion

3.1 Experimental results and discussion

Each region has different wind speeds depending on the season. According to the local meteorological data, the Tabuk region's average wind speeds during the windier months of the year (January through July) exceeded 3.66 m/s, while they were about 3.3 m/s during the calmer months of the year (August through December). The aerodynamic efficiency of the blades typically depends on the wind speed, size, mass, and quantity of wind energy in a particular blade region. The formula is as follows:

$$p_{\mathrm{w}} = \left(\frac{1}{2}\right)\dot{M}V_{\mathrm{w}}^2. \tag{1}$$

Generally, the air mass per second can be formulated as follows:

$$\dot{M} = V_{\mathrm{w}}A\rho, \tag{2}$$

where A is the turbine's swept area and is given as

$$A = L \times D, \tag{3}$$

where L is the blade length and D is the diameter of the turbine. Then, the air mass per second hitting the blades in any given second can be written as

$$\dot{M} = V_{\mathrm{w}} \times D \times L \times \rho. \tag{4}$$

Thus, the power formula

$$p_{\mathrm{w}} = \left(\frac{1}{2}\right) \times (V_{\mathrm{w}}DL\rho) \times V_{\mathrm{w}}^2 \tag{5}$$

with $\rho = 1.255\,\mathrm{kg/m^3}$, $L = 1\,\mathrm{m}$, and $D = 0.72\,\mathrm{m}$. P_{w} can be written as

$$P_{\mathrm{w}} = (0.\,45)^*(V_{\mathrm{w}}^3). \tag{6}$$

To evaluate wind turbine performance, the power coefficient can be written as follows:

$$C_{\mathrm{p}} = \frac{P_{\mathrm{Mech}}}{P_{\mathrm{w}}}. \tag{7}$$

To evaluate the output of the VAWT, the electrical power can be calculated as follows:

$$P_{\mathrm{E}} = V \times I. \tag{8}$$

The mechanical power can be calculated by using the following equation:

$$P_{\mathrm{Mech}} = T \times \omega, \tag{9}$$

where T is the torque and ω is the angular velocity:

$$\omega = \frac{2\pi N}{60}. \tag{10}$$

The tip speed ratio λ is determined by dividing the speed of the tips of the turbine blades by the speed of the wind as follows:

$$\lambda = \frac{V_{\mathrm{b}}}{V_{\mathrm{w}}}. \tag{11}$$

After conducting the required experiments on natural wind speeds in different Tabuk city areas with different levels and at different time durations, the optimal results were regrouped in Table 2.

The performance of the VAWT over all expected tip speed ratios is reported in Table 2. Based on the experiments on VAWT at natural wind speeds, the results are shown in Figure 4. It is observed that C_{p} increases with λ up to its optimum value and then it decreases with a quick rate. The optimum value of $C_{\mathrm{p}} = 0.45$ for $\lambda = 1.94$.

It is observed that the mechanical power increases quadratically with the wind speed, so the wind turbine can reach high mechanical power at high rotor speeds but is limited, as shown in Figure 4, by a tip speed ratio of about 1.94. A sudden jump in the power coefficient values for the tip speed ratios of 1–2 may be due to inaccurate measurements of the mechanical power. The VAWT's electrical generator is a permanent magnet cable-wound synchronous generator. Figure 5 shows that the electrical power increases approximately linearly with increasing wind speed, implying that the wind turbine can achieve high electrical power at high wind speeds.

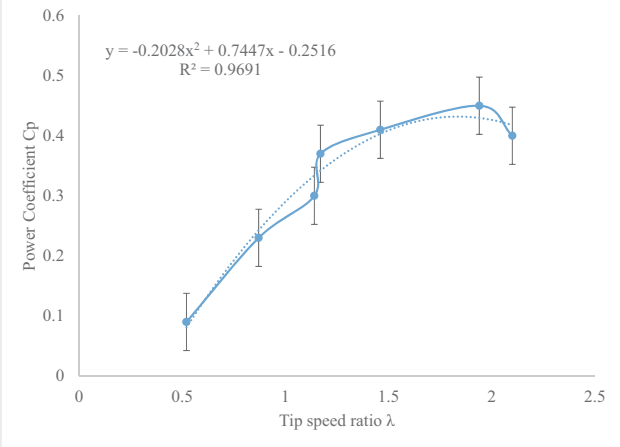

Figure 4: The power coefficient C_p and the tip speed ratio (λ) chart.

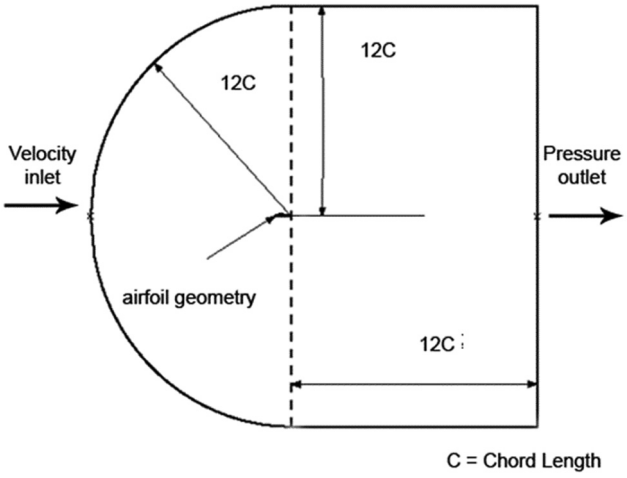

Figure 6: The CFD computational domain and boundary conditions.

3.2 Simulation results and discussion

Generating the right computational domain for the simulation of the airfoil is an important task of the modeling process of the VAWT. Different wind conditions and airfoil profiles were considered. The domain was not too small to correctly reproduce the flow around the airfoil and not too large to avoid unnecessary increases in cell numbers of the grid. An independent study was conducted to select a suitable domain/grid for the present simulation case. The requirements of the meshing in terms of quality and first cell positioning near the airfoil were considered.

Figure 6 shows the CFD computational domain and boundary conditions used to conduct the simulation. The computational domain is composed of an upstream C-shape, half circle, in which the airfoil is included. The airfoil end is located at the center of the semicircle. The diameter of the semicircle is set as 12 times the chord of the airfoil. The downstream domain is a square with a side length equal to the circle diameter. The boundary conditions are defined as follows. The airfoil is simulated as a wall subjected to velocity inlet and pressure outlet boundary conditions. To show the flow field represented by pressure and velocity distributions, the wind velocity was applied horizontally at the cord line and the angles of attack were varied between −9°, 0°, and 9°. Both lift and drag dimensionless coefficients were calculated at 0° angle of attack. As the angle of attack increases, the pressure on the lower side of the airfoil increases while the velocity decreases. With the decrease of the pressure on the upper side of the airfoil, the velocity increases.

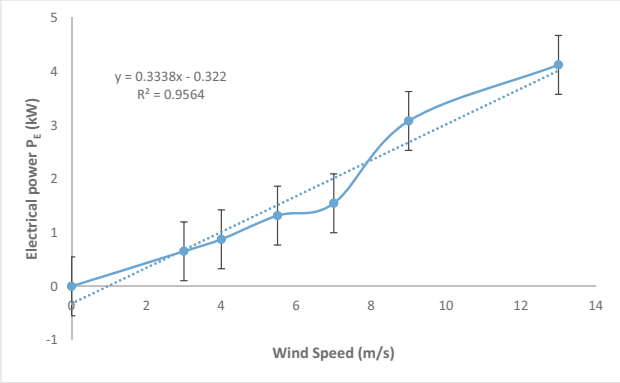

Figure 5: The generated electrical power P_E vs wind speed V_w.

Figure 7 shows a sample of used meshing. The mesh is constructed with Ansys Mesh. The 2-D mapped face meshing, a fine, high smoothing mesh, was constructed with 50 division numbers and a bias factor of about 150. The C–H type structured grid is applied in the airfoil domain to consider the boundary layer effect on the aerodynamic performance of airfoils. Also considering the requirements of the turbulence model for the grid, the boundary layer mesh is denser around the airfoil, so the results met the stability requirements.

Different edges and face sizings are chosen to build different meshes with different numbers of elements to check the independency of the results. As shown in Table 3, five different fine mesh grids were created. The grid with 15,000 cells with about 1.3 h computational time generated the same results as the higher number of cell grids.

The simulation results on pressure coefficients and velocity magnitudes are shown in Figures 8 and 9. The vector representation assigned maximum shear stress zones. The orientation of the blades and the airfoil

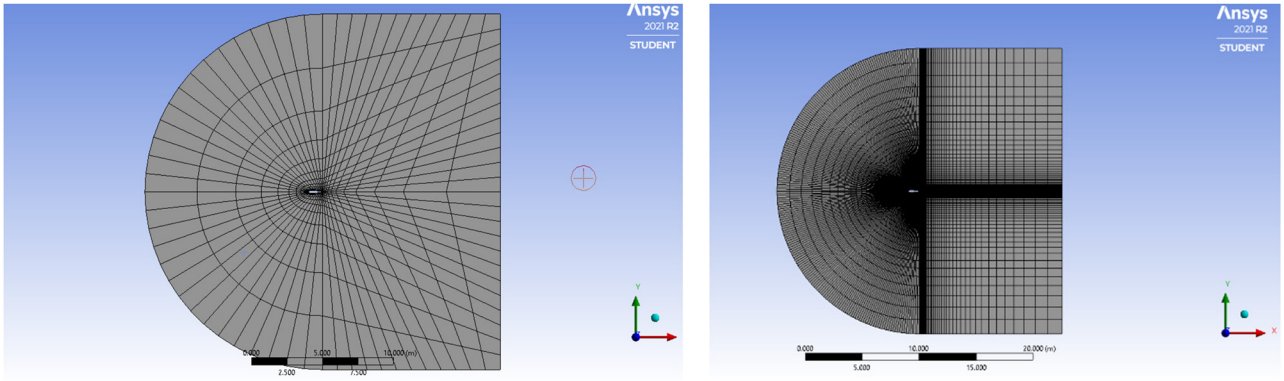

Figure 7: A sample of mesh dependency.

Table 3: Mesh dependency study

Grid	No. of elements	Near-wall mesh quality	Computational time (h)
1	36,000	Satisfied	5.2
2	24,000	Satisfied	3.1
3	15,000	Satisfied	1.3
4	12,000	Not satisfied	1.0
5	9,000	Not satisfied	0.8

positions relative to the angles of attack of the wind helps to have different lift forces from the tail of the airfoil and the front head. The flow field of the trailing edge of the wind turbine blade airfoil shows that the flow still belongs to the laminar status of the different conditions of angles of attack and there is no presence of turbulence. The results of the aerodynamic performance of the blade airfoil using the present model correspond with the experimental results.

The assembly parts, especially the bolts, in the wind turbine are subjected to excessive fatigue loads, and it is crucial to verify and schedule the fixation replacements to prevent premature damage to the wind turbine.

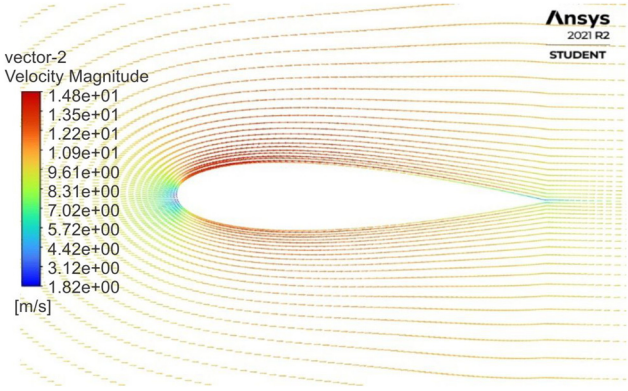

Figure 9: Distribution of velocity magnitude vectors around the airfoil.

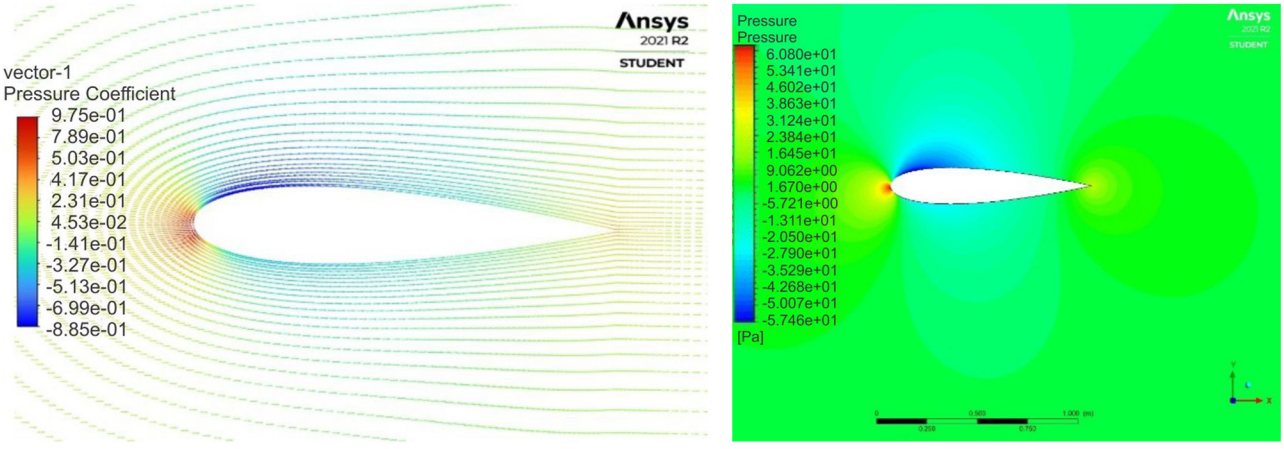

Figure 8: Distribution of pressure coefficient vectors around the airfoil.

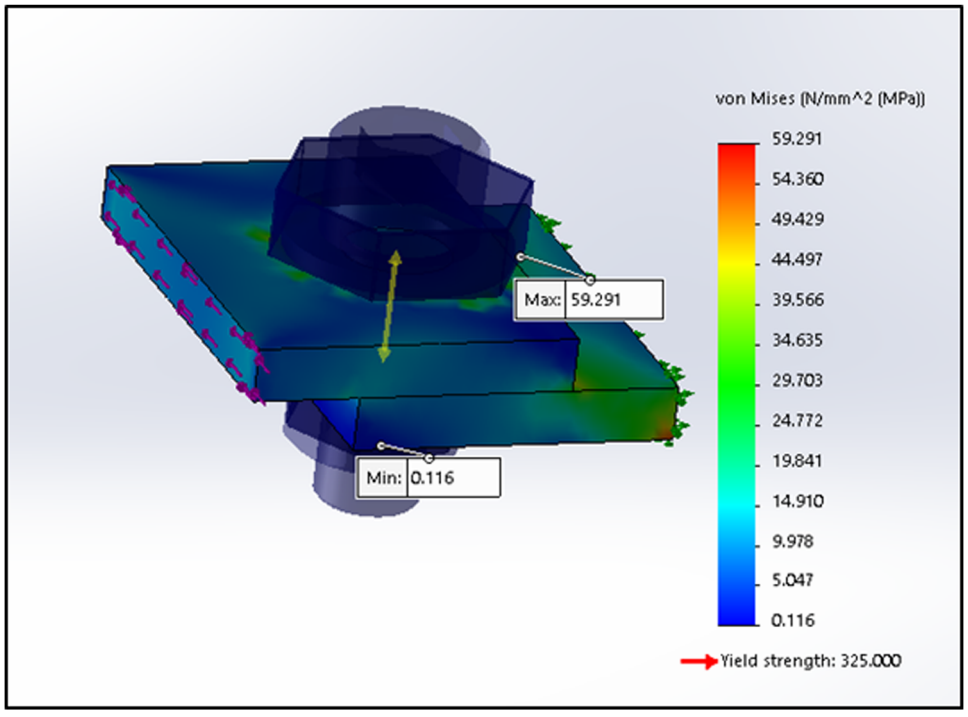

Figure 10: Simulation of shear forces applied at fixation bolts of the wind turbine blades.

The calculation of the radial forces applied to the bolts indicates the level of shear on the bolts and blade materials; the simulation results are shown in Figure 10.

As shown in Figure 10, the zones near the fixation present a high level of stress concentration. Based on the yield strength calculation, the damage and cracking will not take place at the bolts and blade structures.

To compare the experimental results with the simulation, a force simulation was conducted as shown in Figure 11.

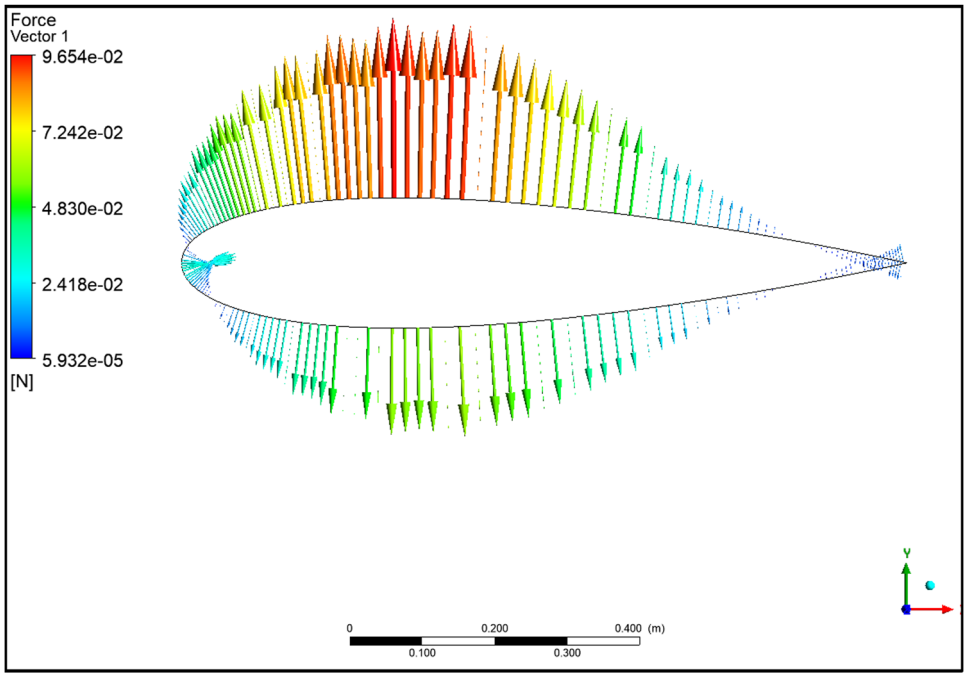

Figure 11: Forces on the airfoil.

The simulation results show a similarity with the experiments on the calculation of the forces on the airfoil; a torque of 3.2 N m at a wind speed of 10 m/s, and a rotor radius of 0.36 m resulted in a force of 8.8 N. The simulation equivalent force was about 2.8 N for a single blade, such as 8.5 N in total, which presents an error of about 3%. The CFD simulation and experimental tests on existing forces confirm that the VAWT structure's resistance can be guaranteed at high wind speeds.

4 Conclusion

Based on the average wind speed in the Tabuk region of Saudi Arabia, the wind turbine was designed with an H-Darrius NACA 0018 airfoil. The turbine was tested in the Tabuk region at different wind speeds. It was observed that the mechanical power increases exponentially with increasing wind speed and so the wind turbine can reach high mechanical power at a high rotor speed. However, a maximum power coefficient of 1.94 corresponds to a rotary speed of about 450 rpm. The electrical power obtained after increasing the input rotary speed of the rotor via the gearbox increases linearly with the wind speed, and the wind turbine can reach high electrical power at high wind speeds. The maximum power coefficient obtained during testing was approximately 0.45 at a tip speed ratio of around 1.94. A verification CFD simulation was conducted on the airfoil at the maximum real-tested wind speed of 10 m/s obtained during experiments. The simulation equivalent force was about 2.8 N for a single blade, such as 8.5 N in total, which presents an error of about 3%. The efficiency of the top-roof VAWT presented in this work is dependent on the presence of a high wind flow.

Conflict of interest: Authors state no conflict of interest.

References

[1] Evans A, Strezov V, Evans JT. Assessment of sustainability indicators for renewable energy technologies. Renew Sustain Energy Rev 13(5):1082–8.

[2] Leijon M, Dahlgren M, Walfridsson L, Ming L, Jaksts A. A recent development in the electrical insulation systems of generators and transformers. IEEE Electr Insul Mag. 2001;17(3):10–5.

[3] Ribrant J, Bertling LM. Survey of failures in wind power systems with focus on Swedish wind power plants during 1997–2005. IEEE Trans Energy Convers. 2007;22(1):167–73.

[4] Jöckel S. Gearless wind energy converters with permanent magnet generators - an option for the future. European Union Wind Energy Conference EWEA. Göteborg, Sweden; 1996. p. 414–7.

[5] Victor M, Ashvinkumar C, Anders G. Performance and wake comparison of horizontal and vertical axis wind turbines. Wind Energy. 2019;22:458–72.

[6] Alexander AD, Marius JS, Tania B. Performance and wake of a Savonius vertical-axis wind turbine under different incoming conditions. Wind Energy. 2019;22:1260–73.

[7] Sander M, Gijs K, Gerard B. Performance of an H-Darrieus in the skewed flow on a roof. J Sol Energy Eng. 2003;125:433–40.

[8] Haraldsdóttir H, Sandström M. Lifetime analysis of a wind turbine component. Gothenburg, Sweden: Chalmers University of Technology; 2016.

[9] Brusca S, Lanzafame R, Messina M. Design of a vertical-axis wind turbine: How the aspect ratio affects the turbine's performance. Int J Energy Environ Eng. 2014;5:333–40.

[10] Tjiu W, Marnoto T, Mat S, Ruslan MH, Sopian K. Darrieus vertical axis wind turbine for power generation I: Assessment of Darrieus VAWT configurations. Renew Energy. 2015;75:50–67.

[11] Gross A, Fase HF, Friederich T, Kloker MJ. Numerical investigation of rotational augmentation for S822 wind turbine airfoil. Wind Energy. 2012;15:983–1007.

[12] Emmanuel OY, Richard O, Albert SK, Muyiwa S. Development of high-performance airfoils for application in small wind turbine power generation. J Energy. 2020;20:1–9.

[13] Bianchini A, Ferrara G, Ferrari L. Design guidelines for H-Darrieus wind turbines: Optimization of the annual energy yield. Energy Convers Manag. 2015;89:690–707.

[14] Migliore P. Comparison of NACA 6-series and 4-digit airfoils for Darrieus wind turbines. J Energy. 1983;7:291–2.

[15] Kline SJ, McClintock FA. Analysis of uncertainty in single-sample experiments. Mech Eng. 1953;75:3–8.

[16] Gherissi A, Ali M. Superficial hardening improvement of nano and micro composite Al/TiC. J Silicate Based Compos Mater. 2019;72:25–9.

[17] Ali M, Gherissi A. Synthesis and characterization of Al-SiO_2 composites. J Ceram Process Res. 2019;20:259–63.

[18] Ali M. Synthesis and characterization of epoxy matrix composites reinforced with various ratios of TiC. Jordan J Mech Ind Eng. 2016;10:231–7.

[19] Allet A, Hallé S, Paraschivoiu I. Numerical simulation of dynamic stall around an airfoil in Darrieus motion. J Sol Energy Eng. 1999;121(1):69–76.

[20] Zhang LX, Liang YB, Liu XH, Jiao QF, Guo J. Aerodynamic performance prediction of straight-bladed vertical axis wind turbine based on CFD. Adv Mech Eng. 2013;5:905379.